APPENDIX A

Pattern for Crystal Model

With a crystal model in your hands you can find halo poles easily (Chapter 14). The pattern below is for a crystal with $\{1\,0\,\bar{1}\,1\}$ pyramid faces and $c/a = 1.63$ as usual. We suggest enlarging the pattern on a photocopier and then constructing the model from cardboard.

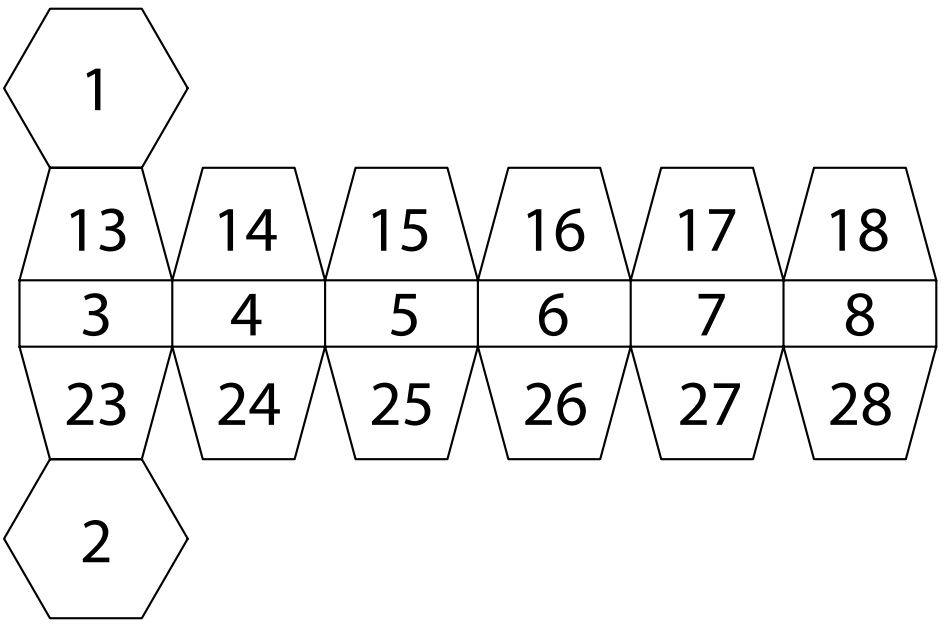

TABLE B.1 Correspondence between some traditional halo names and names derived from the halo classification of Chapters 12–14.

Traditional name	Name from halo classification
Parhelia	22° plate arcs
Tangent arc	22° column arc
Infralateral and supralateral arcs	46° column arcs
Circumzenith arc	Upper symmetric 46° plate (or Parry) arc
Circumhorizon arc	Lower symmetric 46° plate (or Parry) arc
Parry infralateral arcs	Infralateral (46°) Parry arcs
Parry supralateral arcs	Supralateral (46°) Parry arcs

APPENDIX B

Halo Terminology

Halo names arose over time. Some halos, such as the Wegener arc, bear the name of an observer or halo scientist. Others, such as the circumzenith arc, are named according to their location or appearance. When you begin to consider odd radius halos, you soon realize that some sort of more uniform and more conceptual terminology is desirable. Only the most devoted enthusiasts will be able to remember that the halo of van Buijsen, say, is the 9° halo, whereas the halo of Feuillée is the 35° halo.

In this book we therefore introduced a uniform nomenclature scheme for refraction halos, its basis being the halo classification described in Chapters 12–14. In some cases the new scheme resulted in new names for familiar halos. We used the new names when we felt that they added clarity.

We are not, however, suggesting a massive renaming of old halos. Most of the time the circumzenith arc, for example, will continue to be the circumzenith arc rather than the upper symmetric 46° plate (or Parry) arc. But there are times when we get some insight into the circumzenith arc by realizing that it is indeed the upper symmetric 46° plate arc. And surely we understand the upper symmetric 23° plate arc better by recognizing its close relation with the circumzenith arc—a relation that is emphasized by the new nomenclature.

A disadvantage of the new nomenclature is of course that some refraction halos now have more than one name. They are listed in Table B.1.

For the arcs often called the heliac arc and Tricker arc we have instead used the names helic arc and anthelic arc, respectively, in order to stress the tight relation among the helic, anthelic, subhelic, and subanthelic arcs. These two changes do not appear in the table, since they do not pertain to refraction halos.

APPENDIX C

Halo Observation and Photography

Anyone who sees a rare halo can obtain useful photographs. In the case of odd radius halos, the photographs will be more valuable scientifically if angular measurements can be made from the photos, so that halo radii can be measured. In this appendix we offer some general suggestions for halo photography and then some specific precautions that need to be taken so that angular distances can be found from the photos.

When a good halo display comes along, there are no real tricks to getting good photographs of it. Just block the sun with something (but see below) and fire away. Do not stint on film; the display is apt to change from moment to moment, and there are no second chances. Bracket your exposures, especially for wide angle lenses. For lunar displays use a tripod, of course, and try exposures from 5 to 40 seconds with ASA400 film and with the aperture wide open. With a digital camera you can check your photos as you take them, thus reducing the number of different exposure times, but we still recommend some bracketing.

Although there are no major secrets to halo photography, there are of course things that can go wrong. Probably the best advice we can give is to experiment. Don't wait for the big display to test your operation. Get the bugs out by photographing a few mediocre displays that you do not care about.

Your first attempt at halo photography will reveal the huge size of halos and the consequent need for wide angle lenses. A 28mm lens has a wide enough field of view to include both parhelia. A 20mm lens is enough for the entire 22° halo, and a 15mm lens is enough for the supralateral arc. (The preceding numbers are for traditional film cameras; their equivalents for a digital camera can normally be found in the camera manual.) Zoom lenses are not so good if angular measurements are ever to be made from the photographs.

One recommendation specific to digital: Archive the original files and do not tamper with them. Any processing should be done on copies. It is easy to overdo digital enhancement, the result being an ugly photo that may contain artifacts mimicking halos.

While we are on the subject of digital: Digital cameras are vulnerable to cold and condensation. If you anticipate photographing low level halo displays, especially lunar displays, where your camera will be exposed to prolonged cold, an old-fashioned mechanical film camera may be preferable to digital.

What about measuring halo radii from a photo? The ideal halo display for doing so is a lunar display in which stars as well as halos are visible (e.g., Figure 15.4). The main thing then is to **record the time and place of each photo**, so that celestial coordinates of the moon can be found. (If your camera is digital, the time will be included in the EXIF data, which of course should be saved.) The angular distance from the moon to any star can then be calculated. If there are stars in your photo near the halos, you will be able to make some estimates of the halo radii.

But good lunar halo displays are not common, especially ones with lots of stars. So normally you must resort to something like the star triangle method of Appendix D. The method requires some effort, but it will work for any photo, daytime or nighttime. For the photographer the main thing to remember is that **the disk of the sun (or moon) should be clear in the photo**. This means having two pieces of polarizing film available, so that they can be crossed and interposed between the camera and the sun, as in Figure 15.2. Polarizing film is available through many scientific supply companies.

Recently Marko Riikonen has been experimenting with a technique that superposes large numbers of photos of the same halo display. We suspect this is the wave of the future in halo photography. The technique smoothes out inhomogeneities in the clouds so that the halos stand out better against the background, and it reduces any intensity variations in the halos that result from variability in the clouds. The result is a composite image that shows far more than any of its component images and indeed shows far more than would be seen by an observer during the display. Figure C.1 is one of Riikonen's composites. He stresses that the display itself was not outstanding.

Miscellaneous observing suggestions If you have come this far in the book, you will know something about halo observing. We nevertheless remind you to look at the entire sky. That is, do not be completely seduced by the sunward side of the sky; look overhead as well, and look toward the anthelic region. Look at the whole sky.

Some halos are sufficiently polarized so that the polarization can be detected by observing the halos through polarizing film or polarized sunglasses. Try it first

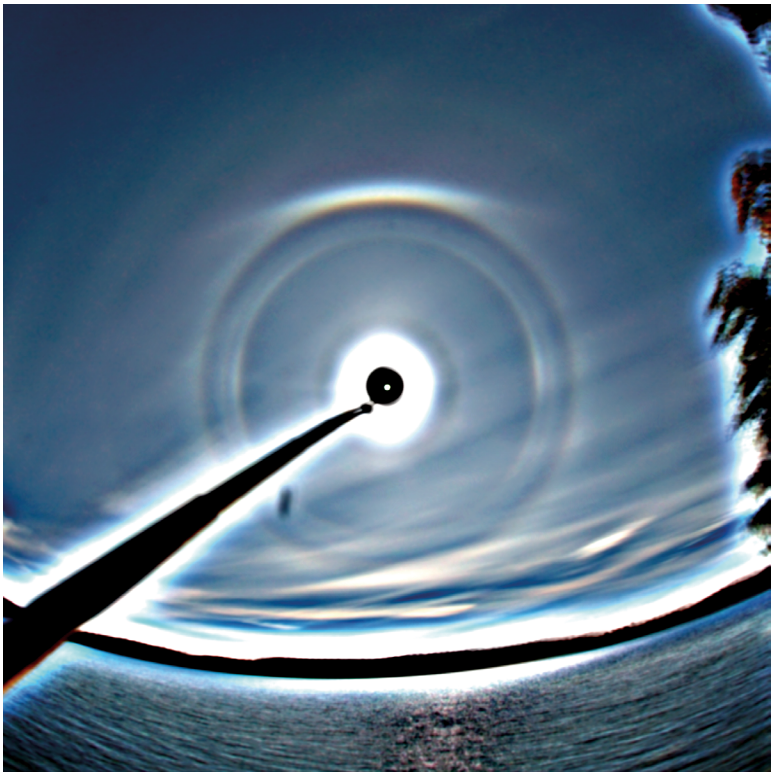

FIGURE C.1 Composite of many images of the same odd radius halo display. Fifty-one photographs, taken over an interval of ten minutes, were enhanced with digital unsharp masking and then superposed to make the composite. The composite shows much more than was visible at the time of the display. Kontiolahti, Finland, August 20, 2005. Photo © Marko Riikonen.

with a bright parhelion. Just observe the parhelion through the polarized glasses and then rotate the glasses ninety degrees. You will see a small horizontal shift in the inner edge of the parhelion.

If you own a digital camera with a polarizing filter, you can try a fancier version of the previous experiment. With the camera mounted on a tripod, zoom in on the parhelion and photograph it first with the polarizer positioned so that the parhelion is closest to the sun, then again so that the parhelion is farthest from the sun. The resulting two photos can then be superimposed and animated to show the shift. (The disadvantage of the traditional film camera here is that aligning the photos can be an ordeal.)

The shift in a halo due to the polarization tells something about the halo, and it can even be decisive in identifying certain odd radius halos. So if you are lucky enough to see a bright odd radius display, try to remember—in the excitement of

the moment—to look for the shift in each halo. If you are able to detect the shift, note in writing which way it goes, and note the corresponding orientation of your polarized glasses. For much more on the role of polarization in halos, including many observational tips, see the article by Können [40]. Können apparently was the first to notice the shift.

If you live in a cold place, you can easily make plastic replicas of atmospheric ice crystals during low level halo displays, and this information, too, can be useful if the halos are exotic. All you need are some glass slides and acrylic spray. We use Krylon clear acrylic spray, which is carried by many hardware and paint stores. When crystals are falling, just spray a slide with the Krylon and then wave it through the air for twenty seconds or so to intercept the crystals. (Both the slide and the Krylon should be cooled before spraying, but the Krylon should not be cooled so much that it comes out of the can in a trickle rather than a spray.) The sprayed slide should be left outside in the cold for an hour to allow the crystals to evaporate. Then the slide can be brought inside and examined with a microscope or strong hand lens. If the halo display is important, we generally make several replica slides, varying the amount of spray from one to the next. Usually the replicas are fairly good, but not always. They are never the equal of photographs of the crystals themselves, but cold weather photography with a microscope is a more demanding project.

At the time of this writing there were organized networks of halo observers in Finland, Germany, Holland, and the Czech Republic. Such networks, with many alert observers spread over large areas, have had a huge impact on halo studies, by providing photographs of rare halo displays that would never have been seen without the networks. These networks welcome new members.

Finally, some obvious but crucial reminders: Watch the sky, and keep the camera, the polarizers, and the replica materials with you.

APPENDIX D

From Pixels to Degrees

Accurate angular measurements of halo radii are central to our story, but getting them turns out to be a challenge. In this appendix we explain how to measure angular distances in a halo photograph, partly so that people can do it for themselves, but mainly to give some confidence in our measurements.

Here we are not concerned with the problem of pinpointing the (always fuzzy) edge of a halo. Instead we imagine that two points on a halo photo have already been specified. The problem is then to find the angular distance between them.

Getting angular distances from a photograph is more complicated than you may imagine. Whereas on a map of New York City, say, you will usually find a scale of miles, you will not find one on a map of North America. That is because on the map of North America the scale of miles changes from point to point. (It changes with direction as well.) A wide angle photograph of the sky is completely analogous to a map of a large region of the earth. There is no single conversion factor from inches (or pixels) on the photo to degrees in the sky. This is seen dramatically in Figure 6.8, where the 22° circular halo appears grossly distorted at the right of the photo. How, then, do we get angular distances from a halo photo?

The star triangle method

The method that we use is the star triangle method. It is based on the fact that celestial coordinates of stars are known—they can be found from astronomical software packages, for example. We superimpose our halo photo on a photo of a star field taken with the same lens as the halo photo. Points in the halo photo can then be treated as if they were points in the star photo. That is, their

"celestial coordinates" can be found from the celestial coordinates of nearby stars. The angular separation between any two points in the halo photo is then easily computed from their celestial coordinates. The actual handling of the photos is best done electronically, that is, by computer; although the method can in principle be carried out physically, in practice it doesn't work.

Figure D.1 is an example. It shows how to find the angular distance between the sun and the upper right purple dot in the halo photo of Figure 16.7. The halo photo has been superimposed on a suitable star photo—the "background

FIGURE D.1 The star triangle method for finding the angular separation between two points in a photo. Here the points are the white dot (at the sun) and the upper right purple dot in the halo photo of Figure 16.7. The halo photo has been placed electronically on a star field photo, and the opacity of the halo photo has been turned down so that the stars are visible; here the halo photo is barely visible on top of the star photo. The "celestial coordinates" of the white dot are found by interpolation from the celestial coordinates of the three nearby stars 1 Gem, ζ Tau, and 126 Tau. The celestial coordinates of the purple dot are similarly found from the celestial coordinates of α Aur, ε Aur, and η Aur. The angular separation of the two dots is then calculated from their celestial coordinates.

photo"—and the opacity of the halo photo has been turned down so that the stars are visible. In the halo photo you can still make out the sun-blocking stick, but not much more. A small "star triangle" has been chosen surrounding the white dot (the sun position); its vertices are the stars 1 Gem, ζ Tau, and 126 Tau, as shown. The pixel coordinates of the three vertex stars and the white dot are found from the photo. These pixel coordinates are then used to calculate the celestial coordinates of the white dot by interpolation from the celestial coordinates of the vertex stars. The celestial coordinates of the purple dot are found the same way, but using the star triangle with vertices α Aur, ϵ Aur, and η Aur. The angular separation between the white and purple dot is then calculated from their celestial coordinates.

We have programmed the computer to do most of the work. Given pixel coordinates for two points in the photo, the computer will find the best star triangle about each point and then proceed as above to find the angular separation between the points. Figure D.2 shows the graphical output of the computer when asked to measure the angular separation between the same white and purple dots as before.

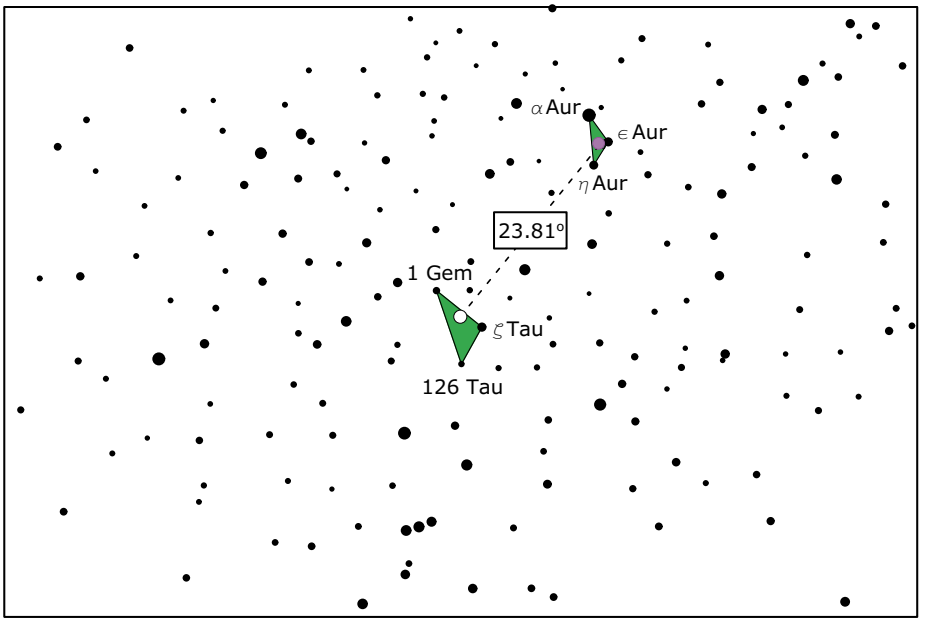

FIGURE D.2 Graphical output of the computer for the angular measurement of Figure D.1. Each black dot is a star in the star field photo. The white dot and the purple dot are the two points whose separation was to be found, the same as in Figure D.1. We had only to measure the pixel coordinates of the two points in the photo, and the computer did the rest: It found the best star triangle (green) for each point, used the star triangles to calculate the celestial coordinates of the two points, and found their angular separation to be 23.81°.

But the computer is not magic, and it needs to be told what stars it has to work with. We must give it pixel coordinates for about 200 stars distributed fairly evenly over the photo.[1] This needs to be done once for each camera lens used in the halo photography. That is, a different background star photo is needed for each lens.

Not just any region of sky will serve as the background photo. Best is a region that is far from the celestial poles and also well above the horizon. Staying away from the poles makes interpolation in star triangles simpler. Staying away from the horizon minimizes distortion from atmospheric refraction. This does not of course eliminate possible distortion in the halo photo due to atmospheric refraction; see page 86.

Checking the star triangle method

How confident can we be in angular separations found by the star triangle method? We believe the method to be accurate to within 0.2°—and usually much better—so long as the points whose separation is to be measured are not too close to the edge of the photo, so long as there are some background stars nearby, and so long as the two photos are carefully aligned.

One way to check the star triangle method is to apply it not to a halo photo but to another star photo. We superimpose the new star photo on the same background star photo as before. The angular separation between two given stars in the new photo can be calculated by using star triangles from the background photo, just as if the new star photo were a halo photo. But the true angular separation between the two stars is of course known, and so the calculated separation can be compared with the true separation.

The upper diagram in Figure D.3 is an example. The black stars are the background stars, the same as in Figure D.1, and the four red stars are from a different star photo. When the black stars are used to compute the angular separations among the four red stars, the six separations are all found to be within 0.13° of their true values; the results are good.

In the lower diagram the photo with the red stars has been offset two millimeters horizontally and one millimeter vertically. (The photos are ordinary 35mm slides.) When the black stars are used as before to calculate the angular separations among the four red stars, some of the resulting separations are now in error by almost two degrees. These errors are far too large if we are trying, say, to identify a halo that could be either the 22°, 23°, or 24° halo. In the star triangle method good alignment of the two photos is crucial.

[1] We could make do with far fewer stars, since we only need background stars in the vicinity of points whose angular separation is to be found. But a large number of stars is preferable, largely for the sake of internal consistency.

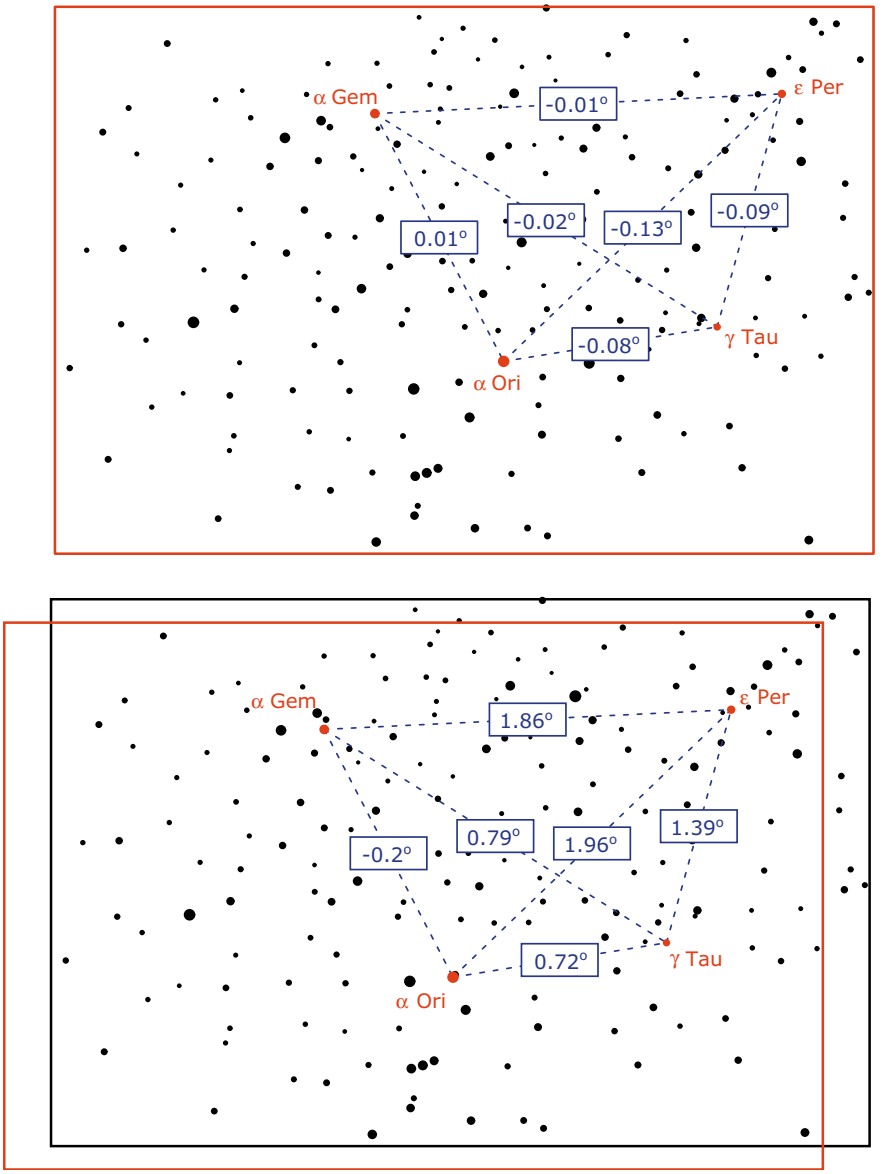

FIGURE D.3 (*Top*) A check of the star triangle method. Instead of a halo photo, another star photo (red stars) was placed on our standard background star photo (black stars). Angular separations among the four red stars were calculated using star triangles from the black stars. The numbers give the errors in the calculated separations—that is, the differences between the calculated values and the true values. (*Bottom*) Same but with a small misalignment of the two photos. The errors in the angular separations are now far too large to be acceptable.

Alignment is trivial for photos taken with a digital camera. With a film camera, however, alignment can be daunting. Both images must be visible in their entirety, right up to the edge where they meet the unexposed, black part of the film (e.g. Figure D.1). This means that slides cannot be scanned in their mounts. It means that the scanner must not crop the images. It means that the sky in the star photo must be light enough so that the edge of the image can be discerned. And so forth. You can now see why the two photos need to be superposed electronically, rather than, say, by projecting them together on a basement wall, as we did for many years, with dismal results.

Avoiding the star triangle method?

Once we have gone to the trouble of measuring pixel coordinates for a large number of stars in the background photo, it does not take much extra effort to understand how the lens works, that is, to understand how angular distances in the sky are related to linear distances in the photo.

If the lens is aimed at the center of a spoked wheel, the wheel will look right when photographed, with the spokes seemingly undistorted. Thus the action that we are trying to capture is radial. For each star we therefore let r and ϕ be the linear and angular distances, respectively, from the star to the center of the photo. The distance r is measured directly from the photo, while ϕ is calculated from the celestial coordinates of the star and the center of the photo, the celestial coordinates of the center being found by the star triangle method. For the stars α Ori and α Aur, for example, the corresponding r and ϕ values are given in the upper diagram of Figure D.4. Expecting that ϕ will be a function of r, we plot the points (r, ϕ) for all of the stars in the diagram. The result is shown in the lower diagram. The curve $\phi(r)$ through the points is what we are after; it tells how points in the sky are related to points in the photo.

Most camera lenses are what is known as rectilinear; with such lenses, straight lines on an object will appear straight in the photo. For a perfectly rectilinear lens the dependence of ϕ on r is given by what we will call the rectilinear approximation, namely,

$$r = f \tan \phi, \tag{D.1}$$

where f is the focal length of the lens. The star photo depicted in Figure D.4 was made with a 20mm lens. With $f = 20$mm, the rectilinear approximation [Eq. (D.1)] indeed comes very close to describing the curve through the plotted points in the figure.[2] But is it close enough so that in measuring angular distances

[2] The curve in the figure is not that given by Eq. (D.1) but is a fourth degree polynomial chosen to best fit the plotted points.

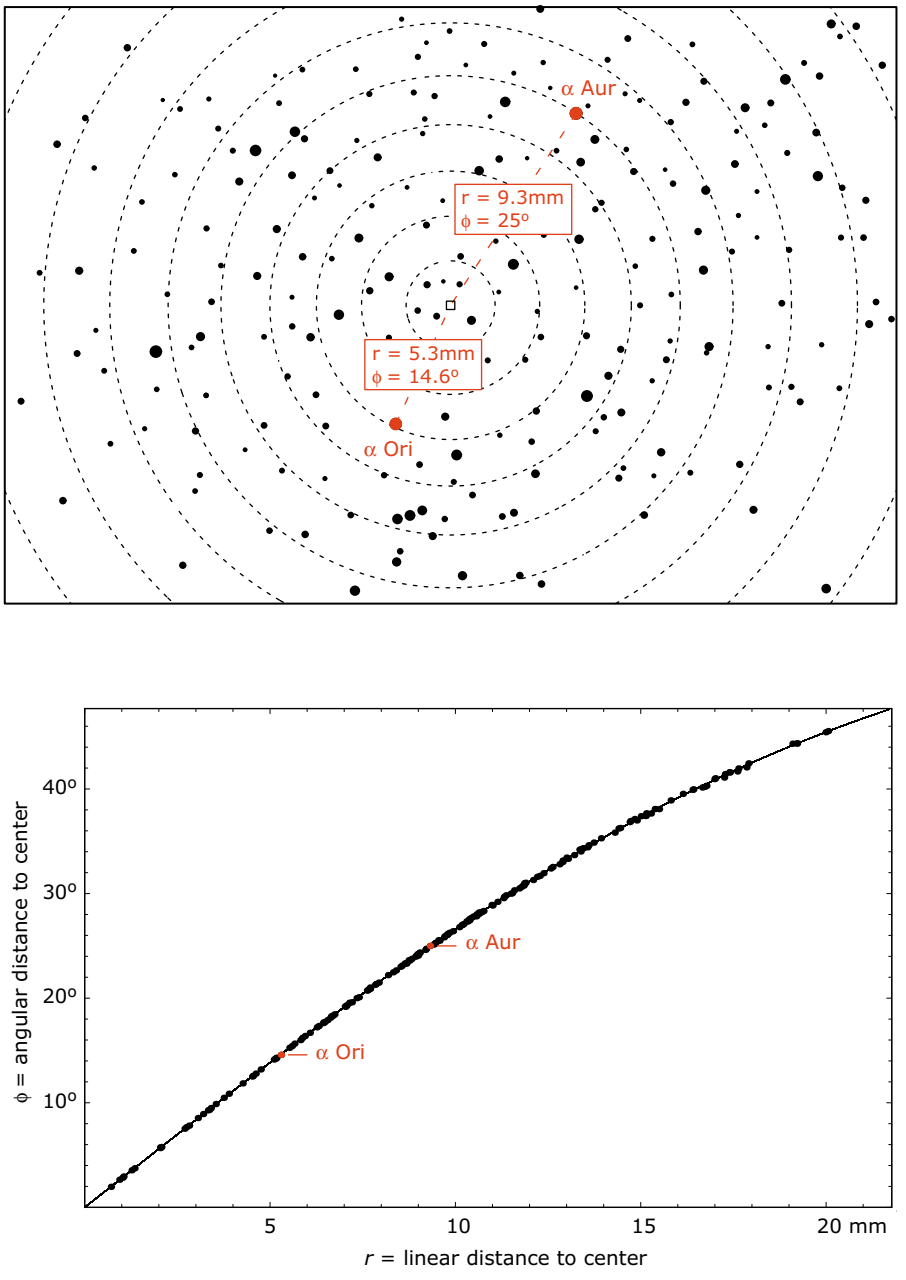

FIGURE D.4 (*Top*) Stars from the same background photo as in Figures D.1, D.2, and D.3. For the two stars α Ori and α Aur the linear distance r and angular distance φ to the center of the photo are given. The dashed circles are at $\varphi = 5°, 10°, 15°\ldots$. (*Bottom*) The same stars but with each star plotted at its corresponding point (r, φ). The curve $\varphi(r)$ through these points describes the behavior of the lens.

we can use the rectilinear approximation and dispense with the star triangle method? If we use the rectilinear approximation to find the angular separation between two stars, we find that we can get errors up to about half a degree. (Stars near opposite corners of the photo give errors of about a degree, but this is the worst case, and it is not a case that would be expected to arise in measuring halo photos.) Half degree errors are too much for our purposes, especially since we always have to contend with an additional uncertainty of half a degree or more in locating the halo edge. So for our 20mm lens the rectilinear approximation is not good enough. For other lenses the rectilinear approximation may be better or worse, but it is hard to know in advance how good it will be, since lens manufacturers are reluctant to divulge this information. We seem to be stuck with something like the star triangle method.

APPENDIX E

More Crystallography

This appendix contains derivations of the crystallographic facts that were used in Chapters 7, 9, and 11. In discussing crystallography, our only goal is to get some idea of what faces might be likely on an ice crystal. What we present here is therefore only a fragment of the subject of crystallography as a whole. For much more see the books by Buerger [11] and Senechal [67].

Lattice, basis, dual basis

Associated with a crystal is a 3-dimensional *lattice,* which consists of all integral linear combinations $n_1\mathbf{v}_1 + n_2\mathbf{v}_2 + n_3\mathbf{v}_3$ of three independent vectors $\mathbf{v}_1$, $\mathbf{v}_2$, $\mathbf{v}_3$ in 3-space. The vectors $\mathbf{v}_1$, $\mathbf{v}_2$, $\mathbf{v}_3$ are a *lattice basis* for the lattice.

A *lattice plane* is a plane that passes through three non-collinear lattice points. Thinking of the lattice points as sites where atoms can be added to the crystal during its growth, we regard the lattice planes as being the possible crystal faces. Not all of the lattice planes, however, are equally likely. All else being equal,[1] the likelihood of a lattice plane being (parallel to) a crystal face is thought to depend on the density of lattice points on it. Equivalently, the likelihood depends on the spacing between the lattice plane and the adjacent parallel lattice plane; the larger the spacing, the more likely the crystal face.[2]

[1] All else would *not* be equal if, for instance, the internal structure of the crystal had low symmetry. Ice, however, seems to have full hexagonal symmetry, see page 115.

[2] The principle that likelihood should increase with lattice spacing is known as Bravais' law. This is not the same as the Bravais' law of classical halo theory [31, pp 504–508]. The latter is now mainly of historical interest and is an easy consequence of our geometrical version of the law of refraction (page 38).

The *dual basis* vectors $\mathbf{w}^1$, $\mathbf{w}^2$, $\mathbf{w}^3$ will be the key to handling lattice planes and hence crystal faces. The dual basis vectors are defined by

$$\mathbf{w}^i \cdot \mathbf{v}_j \;=\; \delta^i_j \;=\; \begin{cases} 1 & \text{if } i = j \\ 0 & \text{if } i \neq j \end{cases} \tag{E.1}$$

The dual basis for ice is calculated at the end of this appendix.

Planes

A plane, whether a lattice plane or not, is determined by its normal vector $\mathbf{N}$ and by a point $\mathbf{p}_0$ on the plane. Like any vector, the normal vector can be written $\mathbf{N} = h\mathbf{w}^1 + k\mathbf{w}^2 + l\mathbf{w}^3$ for some real numbers h, k, and l. A point $\mathbf{p} = x\mathbf{v}_1 + y\mathbf{v}_2 + z\mathbf{v}_3$ is on the plane if and only if the vector from $\mathbf{p}_0$ to $\mathbf{p}$ is perpendicular to $\mathbf{N}$:

$$\begin{aligned} 0 &= \mathbf{N} \cdot (\mathbf{p} - \mathbf{p}_0) \\ &= \mathbf{N} \cdot \mathbf{p} \;-\; \mathbf{N} \cdot \mathbf{p}_0 \\ &= \left(h\mathbf{w}^1 + k\mathbf{w}^2 + l\mathbf{w}^3\right) \cdot (x\mathbf{v}_1 + y\mathbf{v}_2 + z\mathbf{v}_3) \;-\; \mathbf{N} \cdot \mathbf{p}_0 \\ &= hx + ky + lz \;-\; \mathbf{N} \cdot \mathbf{p}_0 \end{aligned} \tag{E.2}$$

That is, the equation of the plane is

$$hx + ky + lz = d, \tag{E.3}$$

where $d = \mathbf{N} \cdot \mathbf{p}_0$. We stress that x, y, z are the coordinates of $\mathbf{p}$ with respect to $\mathbf{v}_1$, $\mathbf{v}_2$, $\mathbf{v}_3$, and that h, k, l are the coordinates of $\mathbf{N}$ with respect to $\mathbf{w}^1$, $\mathbf{w}^2$, $\mathbf{w}^3$.

Lattice planes and Miller indices

The equation of a plane not containing the origin can be written $h'x + k'y + l'z = 1$. If the plane is a lattice plane, then it contains three independent lattice points $\mathbf{p}_1$, $\mathbf{p}_2$, $\mathbf{p}_3$, where $\mathbf{p}_i = x_i\mathbf{v}_1 + y_i\mathbf{v}_2 + z_i\mathbf{v}_3$ for some integers x_i, y_i, z_i. Then

$$h'x_i + k'y_i + l'z_i = 1, \quad i = 1, 2, 3. \tag{E.4}$$

Solving these three linear equations for h', k', l' using, say, Cramer's Rule, shows that h', k', l' are rational and that the plane equation can therefore be rewritten $h''x + k''y + l''z = n''$, where h'', k'', l'', n'' are integers and $n'' > 0$. Since $\mathbf{p}_1$ is on the plane, then $h''x_1 + k''y_1 + l''z_1 = n''$. The integer n'' must therefore be divisible by the greatest common divisor of h'', k'', l''. Dividing both sides of the plane equation by the greatest common divisor gives $hx + ky + lz = n$, where n is a positive integer and h, k, l are relatively prime integers.

Conversely, if h, k, l are relatively prime integers, then there are integers x_1, y_1, z_1 such that $hx_1 + ky_1 + lz_1 = 1$ [52, page 5]. The lattice point $\mathbf{p}_1 = x_1\mathbf{v}_1 + y_1\mathbf{v}_2 + z_1\mathbf{v}_3$ is therefore on the plane $hx + ky + lz = 1$. So are the two lattice points $\mathbf{p}_2 = \mathbf{p}_1 + k\mathbf{v}_1 - h\mathbf{v}_2$ and $\mathbf{p}_3 = \mathbf{p}_1 + l\mathbf{v}_1 - h\mathbf{v}_3$, and if $h \neq 0$, as we can assume without loss of generality, then $\mathbf{p}_1$, $\mathbf{p}_2$, $\mathbf{p}_3$ are non-collinear, since $(\mathbf{p}_2 - \mathbf{p}_1) \times (\mathbf{p}_3 - \mathbf{p}_1) \neq \mathbf{0}$. Thus $hx + ky + lz = 1$ is a lattice plane. And so is the plane $hx + ky + lz = n$ since it contains the three non-collinear lattice points $n\mathbf{p}_1$, $n\mathbf{p}_2$, $n\mathbf{p}_3$. Thus:

Criterion for lattice plane *A plane not containing the origin is a lattice plane if and only if its equation can be written*

$$hx + ky + lz = n \tag{E.5}$$

for some relatively prime integers h, k, l and some positive integer n.

The integers h, k, l are known as the *Miller indices* of the plane. The vector $\mathbf{N} = h\mathbf{w}^1 + k\mathbf{w}^2 + l\mathbf{w}^3$ is the outward normal to the plane, and the point $\mathbf{p} = x\mathbf{v}_1 + y\mathbf{v}_2 + z\mathbf{v}_3$ with x, y, z satisfying Eq. (E.5), is a typical point on the plane.

To get a more concrete feeling for Miller indices, notice that the lattice plane $hx + ky + lz = 1$, which has Miller indices h, k, l, passes through the three points $(1/h)\mathbf{v}_1$, $(1/k)\mathbf{v}_2$, and $(1/l)\mathbf{v}_3$. Figure 9.4 illustrates this remark with three examples.

As explained on page 97, Miller indices for ice crystals are usually given as 4-tuples rather than triples.

Spacing of lattice planes

If the Miller indices h, k, l are fixed and if n takes on all positive integral values, then Eq. (E.5), or the equivalent equation $\mathbf{N} \cdot \mathbf{p} = n$, generates all lattice planes having the given Miller indices. The planes are parallel and equally spaced. The spacing between two adjacent planes $\mathbf{N} \cdot \mathbf{p} = n$ and $\mathbf{N} \cdot \mathbf{p} = n + 1$ can be found by taking points $\mathbf{p}_1$ and $\mathbf{p}_2$ on the respective planes and then projecting $\mathbf{p}_2 - \mathbf{p}_1$ onto $\mathbf{N}$. The projection is

$$\frac{\mathbf{N} \cdot (\mathbf{p}_2 - \mathbf{p}_1)}{|\mathbf{N}|} = \frac{\mathbf{N} \cdot \mathbf{p}_2 - \mathbf{N} \cdot \mathbf{p}_1}{|\mathbf{N}|} = \frac{n + 1 - n}{|\mathbf{N}|} = \frac{1}{|h\mathbf{w}^1 + k\mathbf{w}^2 + l\mathbf{w}^3|},$$

that is,

$$\text{lattice plane spacing} \;=\; \frac{1}{|h\mathbf{w}^1 + k\mathbf{w}^2 + l\mathbf{w}^3|} \tag{E.6}$$

Earlier we claimed that spacing is correlated with likelihood; the larger the lattice plane spacing, the more likely the crystal face. Table E.1 gives lattice plane spacings for the mineral beryl. Paradoxically, we know more about polyhedral beryl crystals than we do about polyhedral ice crystals. Since we know what the common faces on real beryl crystals are, we can use the table as a partial test of the correlation between spacing and likelihood. From the table it appears that the correlation is good but not perfect.

Table E.2 is the same but for ice instead of beryl. The table should give an indication of what ice crystal faces are likely.[3] Only the three most likely faces—in the top three rows of the table—are known to occur.

In earlier chapters we said that the crystal faces with small Miller indices are most likely. That needs qualification. A given lattice will always have many possible lattice bases. Changing from one lattice basis to another will change the Miller indices of a lattice plane, so that a plane with small Miller indices might become a plane with large Miller indices. The plane itself does not change, and neither does the lattice plane spacing. It is the spacing, not the Miller indices, that is the indication of likelihood. For the usual choice of basis, however, large spacing does indeed correspond to small Miller indices, as we said.

Sunagawa [73] has a much more sophisticated discussion of the question of what crystal faces are likely.

Inclination angle *x*

Let $\mathbf{v}_1$, $\mathbf{v}_2$, $\mathbf{v}_3$ be our usual lattice basis for ice, and orient the basis so that $\mathbf{v}_3$ is vertical, as in Figure 9.3. For a plane with Miller indices hkl the inclination angle x is then the angle between the plane and a vertical line, which is the same as the angle between its normal $\mathbf{N} = h\mathbf{w}^1 + k\mathbf{w}^2 + l\mathbf{w}^3$ and a horizontal plane. But from Eq. (E.1) we know that $\mathbf{w}^1$ and $\mathbf{w}^2$ are horizontal, and $\mathbf{w}^3$ is vertical, so

$$\tan x = \frac{|l\mathbf{w}^3|}{|h\mathbf{w}^1 + k\mathbf{w}^2|} \tag{E.7}$$

Then from Eq. (E.11),

[3] Even without the beryl table, it is clear that spacing is only loosely correlated with likelihood. In Table E.2, for ice, the spacing values for the $\{1\,0\,\bar{1}\,0\}$ prism faces and the $\{1\,0\,\bar{1}\,1\}$ pyramid faces are nearly the same, yet the former faces are far more common than the latter. And pyramid faces are much more common on small ice crystals than on large ones, yet the spacing should be the same for both, since it is an internal feature.

$$\tan x \;=\; \frac{\sqrt{3}}{2}\,\frac{a}{c}\,\sqrt{\frac{l^2}{h^2+hk+k^2}} \tag{E.8}$$

Also see Figures 9.9 and 9.10, which are the special cases $k = 0$ and $h = k$.

Rational Tangents Principle *Suppose* $\tan x/\tan x_0 = v/u$ *for some small positive integers* u *and* v*. Then if* x_0 *is a crystallographically likely inclination angle, so is* x*.*

To see why this should be so, observe that if face $h\,k\,l$ has inclination x_0, then from Eq. (E.7) the face $uh\,uk\,vl$ has inclination x, where $\tan x = (v/u)\tan x_0$. And if h, k, l, u, v are all small integers, then so are uh, uk, vl.[4]

The Rational Tangents Principle is obviously vague, just as "small" is vague.

Calculation of the dual basis

Given a basis $\mathbf{v}_1$, $\mathbf{v}_2$, $\mathbf{v}_3$ we still need to find its dual basis, that is, the basis $\mathbf{w}^1$, $\mathbf{w}^2$, $\mathbf{w}^3$ satisfying Eq. (E.1). Letting

$$\mathbf{w}^i = \sum_{k=1}^{3} g^{ik}\mathbf{v}_k \tag{E.9}$$

and taking the dot product of both sides of the equation with $\mathbf{v}_j$ gives $\delta^i_j = \sum g^{ik}g_{kj}$, where $g_{kj} = \mathbf{v}_k \cdot \mathbf{v}_j$. Thus the matrix (g^{ij}) is the inverse of the matrix (g_{ij}). Taking the dot product with $\mathbf{w}^j$ instead of $\mathbf{v}_j$ gives $g^{ij} = \mathbf{w}^i \cdot \mathbf{w}^j$.

For our usual lattice basis for ice (Figure 9.3),

$$(g_{ij}) = \begin{pmatrix} \mathbf{v}_1\cdot\mathbf{v}_1 & \mathbf{v}_1\cdot\mathbf{v}_2 & \mathbf{v}_1\cdot\mathbf{v}_3 \\ \mathbf{v}_2\cdot\mathbf{v}_1 & \mathbf{v}_2\cdot\mathbf{v}_2 & \mathbf{v}_2\cdot\mathbf{v}_3 \\ \mathbf{v}_3\cdot\mathbf{v}_1 & \mathbf{v}_3\cdot\mathbf{v}_2 & \mathbf{v}_3\cdot\mathbf{v}_3 \end{pmatrix} = \begin{pmatrix} a^2 & \frac{-a^2}{2} & 0 \\ \frac{-a^2}{2} & a^2 & 0 \\ 0 & 0 & c^2 \end{pmatrix} \tag{E.10}$$

$$\begin{pmatrix} \mathbf{w}^1\cdot\mathbf{w}^1 & \mathbf{w}^1\cdot\mathbf{w}^2 & \mathbf{w}^1\cdot\mathbf{w}^3 \\ \mathbf{w}^2\cdot\mathbf{w}^1 & \mathbf{w}^2\cdot\mathbf{w}^2 & \mathbf{w}^2\cdot\mathbf{w}^3 \\ \mathbf{w}^3\cdot\mathbf{w}^1 & \mathbf{w}^3\cdot\mathbf{w}^2 & \mathbf{w}^3\cdot\mathbf{w}^3 \end{pmatrix} = \big(g^{ij}\big) = (g_{ij})^{-1} = \begin{pmatrix} \frac{4}{3a^2} & \frac{2}{3a^2} & 0 \\ \frac{2}{3a^2} & \frac{4}{3a^2} & 0 \\ 0 & 0 & \frac{1}{c^2} \end{pmatrix} \tag{E.11}$$

[4] The integers $uh\,uk\,vl$ might not be relatively prime, but they can be made so by dividing through by their greatest common divisor, and this does not change the argument.

TABLE E.1 Spacing and inclination angle x for lattice planes of the mineral beryl. Lattice planes are given by their Miller indices and are listed in order of decreasing spacing. The five rows marked as common are the five crystallographic forms for beryl given in *Dana's Manual of Mineralogy* [32]. The fact that they appear near the top of the list suggests that there is indeed some correlation between spacing and likelihood; the larger the spacing, the greater the likelihood of getting a beryl crystal face having the given Miller indices. The spacing values are calculated from Eq. (E.6) and then normalized so that the largest is unity. Angle x is calculated from Eq. (E.8). The internal symmetry of beryl is similar to that of ice, but with $c/a = 0.9975$.

Indices	Spacing	Angle x	Form	
0001	1.000	90.0°	basal	(most common)
$10\bar{1}0$	.868	0.0	hex prism I	(most common)
$10\bar{1}1$	.656	41.0	hex dipyramid I	
$11\bar{2}0$	.501	0.0	hex prism II	(less common)
$11\bar{2}1$	.448	26.6	hex dipyramid II	
$10\bar{1}2$	.433	60.1	hex dipyramid I	(less common)
$20\bar{2}1$	.398	23.5	hex dipyramid I	
$11\bar{2}2$	.354	45.1	hex dipyramid II	(less common)
$21\bar{3}0$	.328	0.0	dihex prism	
$21\bar{3}1$	.312	18.2	dihex dipyramid	
$10\bar{1}3$	.311	69.0	hex dipyramid I	
$30\bar{3}1$	.278	16.1	hex dipyramid I	
$11\bar{2}3$	.278	56.4	hex dipyramid II	
...	...	...		

TABLE E.2 Spacing and angle *x* for lattice planes of ice. This table is similar to Table E.1 but with *c/a* = 1.63, the modern value for the *c/a* ratio of ice. The spacing is thought to give a rough indication of the likelihood of getting an ice crystal face having the given Miller indices; the larger the spacing, the more likely the face. The table suggests that Steinmetz and Weickmann were using the most likely pyramid faces but that Humphreys was resorting to highly unlikely crystal faces (Chapter 11).

Indices	Spacing	Angle *x*	Form	
0001	1.000	90.0°	basal	
$10\bar{1}0$	.531	0.0	hex prism I	
$10\bar{1}1$	.469	28.0	hex dipyramid I	(Steinmetz and Weickmann)
$10\bar{1}2$	.364	46.7	hex dipyramid I	
$11\bar{2}0$	.307	0.0	hex prism II	
$11\bar{2}1$	.293	17.1	hex dipyramid II	
$10\bar{1}3$	.282	57.9	hex dipyramid I	
$11\bar{2}2$	.261	31.5	hex dipyramid II	
$20\bar{2}1$	.257	14.9	hex dipyramid I	
$10\bar{1}4$	.226	64.8	hex dipyramid I	
$11\bar{2}3$	.226	42.6	hex dipyramid II	
$20\bar{2}3$	.208	38.6	hex dipyramid I	
$21\bar{3}0$	.201	0.0	dihex prism	
$21\bar{3}1$	.197	11.4	dihex dipyramid	
$11\bar{2}4$	.194	50.8	hex dipyramid II	
$10\bar{1}5$	.187	69.4	hex dipyramid I	
$21\bar{3}2$	.186	21.9	dihex dipyramid	
$30\bar{3}1$	.174	10.0	hex dipyramid I	
$21\bar{3}3$	.172	31.1	dihex dipyramid	
$11\bar{2}5$	.168	56.9	hex dipyramid II	
$30\bar{3}2$	.167	19.5	hex dipyramid I	
$20\bar{2}5$	.160	53.0	hex dipyramid I	
$10\bar{1}6$	.159	72.6	hex dipyramid I	
$21\bar{3}4$	.157	38.8	dihex dipyramid	
$22\bar{4}1$	.152	8.7	hex dipyramid II	
$31\bar{4}0$	.147	0.0	dihex prism	
$11\bar{2}6$	.146	61.5	hex dipyramid II	
$31\bar{4}1$	.146	8.4	dihex dipyramid	
$30\bar{3}4$	.145	35.3	hex dipyramid I	
$21\bar{3}5$	.142	45.1	dihex dipyramid	
$31\bar{4}2$	.141	16.4	dihex dipyramid	
$22\bar{4}3$	.139	24.7	hex dipyramid II	(Humphreys)
...	...	...		
$40\bar{4}3$	.123	21.7	hex dipyramid I	(Humphreys?)

TABLE E.3 Same as Table E.2 except that here $c/a = \sqrt{3/8} = 0.612$, the value for which the Clarke rhombohedral faces are the $\{10\bar{1}1\}$ faces. Names in parentheses indicate whether Bravais, Besson, or Visser used faces with the given Miller indices to explain odd radius halos (Chapter 11).

Indices	Spacing	Angle *x*	Form	
$10\bar{1}0$	1.000	0.0°	hex prism I	
0001	.707	90.0	basal	
$11\bar{2}0$	.577	0.0	hex prism II	
$10\bar{1}1$	.577	54.7	hex dipyramid I	(Bravais, Visser)
$11\bar{2}1$	.447	39.2	hex dipyramid II	
$20\bar{2}1$	.408	35.3	hex dipyramid I	(Visser)
$21\bar{3}0$	.378	0.0	dihex prism	
$21\bar{3}1$	.333	28.1	dihex dipyramid	
$10\bar{1}2$	.333	70.5	hex dipyramid I	(Bravais, Visser)
$30\bar{3}1$	.302	25.2	hex dipyramid I	(Besson, Visser)
$11\bar{2}2$	.302	58.5	hex dipyramid II	
$31\bar{4}0$	.277	0.0	dihex prism	
$22\bar{4}1$	.267	22.2	hex dipyramid II	
$31\bar{4}1$	.258	21.4	dihex dipyramid	
$21\bar{3}2$	.258	46.9	dihex dipyramid	
$30\bar{3}2$	.243	43.3	hex dipyramid I	(Bravais, Visser)
$40\bar{4}1$	.236	19.5	hex dipyramid I	(Visser)
$32\bar{5}0$	.229	0.0	dihex prism	
$10\bar{1}3$	.229	76.7	hex dipyramid I	
$41\bar{5}0$	.218	0.0	dihex prism	
$32\bar{5}1$	.218	18.0	dihex dipyramid	
$31\bar{4}2$	.218	38.1	dihex dipyramid	
$11\bar{2}3$	.218	67.8	hex dipyramid II	
$20\bar{2}3$	.213	64.8	hex dipyramid I	(Visser)
$41\bar{5}1$	.209	17.2	dihex dipyramid	
$21\bar{3}3$	.200	58.1	dihex dipyramid	
$50\bar{5}1$	.192	15.8	hex dipyramid I	
$32\bar{5}2$	.192	33.0	dihex dipyramid	
$41\bar{5}2$	.186	31.7	dihex dipyramid	
$33\bar{6}1$	.186	15.2	hex dipyramid II	
$42\bar{6}1$	.183	15.0	dihex dipyramid	
$22\bar{4}3$	.183	50.8	hex dipyramid II	
$51\bar{6}0$	.180	0.0	dihex prism	
$31\bar{4}3$	.180	49.6	dihex dipyramid	
$51\bar{6}1$	.174	14.3	dihex dipyramid	
$50\bar{5}2$	.174	29.5	hex dipyramid I	
$10\bar{1}4$	.174	80.0	hex dipyramid I	(Bravais, Visser)
$40\bar{4}3$	.171	46.7	hex dipyramid I	(Visser)
...	...	...		
$30\bar{3}4$	.156	62.1	hex dipyramid I	(Visser)
...	...	...		
$80\bar{8}1$	.123	10.0	hex dipyramid I	(Visser)
...	...	...		
$80\bar{8}3$	.110	27.9	hex dipyramid I	(Visser)

APPENDIX F

Living on the (w)Edge

Understanding a halo is sometimes easier from the perspective of the halo-making wedge—this is the insight that underlies the theory of halo poles. In this appendix we use it to show how the pole of a halo determines its contact points, as described in Chapters 14 and 16.

We think of a halo as being generated in a wedge as the wedge takes on various orientations. The following points (vectors) are relevant. Each can be thought of either as a point on the unit sphere, or as an arrow of length one, as explained in Figure 14.1.

- **k** The zenith point, that is, the point overhead.
- **S** The sun point. It is the light point of the entry ray to the wedge.
- **H** The halo point. It is the light point of the exit ray from the wedge.
- **D, E** The minimum deviation entry and exit points, respectively. They are the light points of the entry and exit rays for the minimum deviation ray path (Figure F.1).
- **P** The spin vector (Chapter 13).

We imagine an observer riding on the wedge as it tumbles through space, and we try to visualize the process of halo formation as seen by the wedge rider. We distinguish between a point as seen normally and the same point as seen by the wedge rider; if the former point is written $\mathbf{V}$, the latter is written $\mathbf{V}_u$. The subscript u refers to the wedge orientation.

What is the relation between $\mathbf{V}$ and $\mathbf{V}_u$ at a particular moment? To the wedge rider, the wedge always looks the same, regardless of the motion of the wedge; to be definite, let's assume that the wedge rider always sees the wedge in standard orientation (Figure 14.2). To see the world as the wedge rider sees it, you therefore

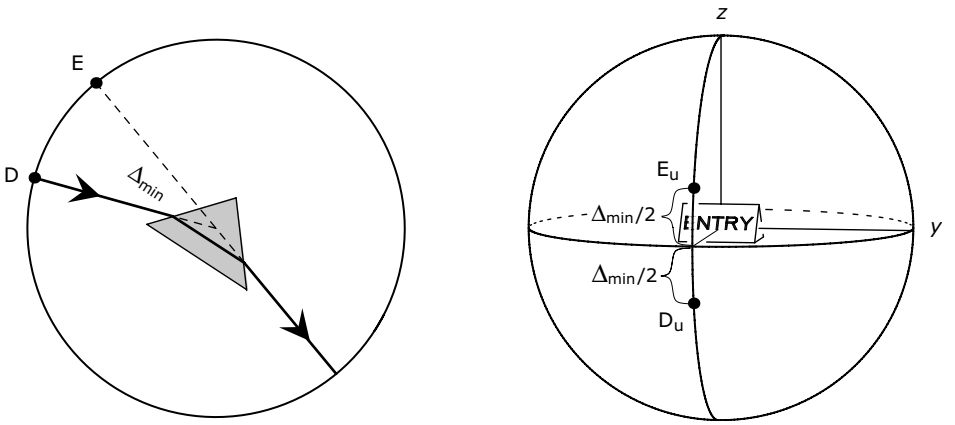

FIGURE F.1 (*Left*) Minimum deviation ray path and minimum deviation entry and exit points **D** and **E** on the unit sphere. (*Right*) The corresponding points $\mathbf{D}_u$ and $\mathbf{E}_u$. They represent **D** and **E** as seen from the wedge. To get $\mathbf{D}_u$ and $\mathbf{E}_u$ from **D** and **E**, you reorient the entire configuration at left so that the wedge ends up in standard orientation, as shown at the right. Comparison of the two diagrams shows that $\mathbf{D}_u$ and $\mathbf{E}_u$ are located on the meridian $y = 0$ at angles of $\Delta_{min}/2$ above and below the equator.

need to reorient yourself so that the wedge appears in standard orientation. Equivalently—and this is what we choose to do—you can instead leave yourself alone and reorient the world so that the wedge is in standard orientation. Thus to get $\mathbf{V}_u$ from $\mathbf{V}$, you imagine the vector $\mathbf{V}$ to be linked rigidly to the wedge, and you then rotate the entire assembly—vector and wedge—in such a way that the wedge ends up in standard orientation. Wherever $\mathbf{V}$ ends up—that is $\mathbf{V}_u$. Figure 14.3 illustrated $\mathbf{V}_u$ for $\mathbf{V} = \mathbf{P}$. Thus when we found the pole $\mathbf{P}_u$ of the halo, we put the wedge in standard orientation; where the spin vector $\mathbf{P}$ ended up—that was $\mathbf{P}_u$. Figure F.1 illustrates $\mathbf{V}_u$ for $\mathbf{V} = \mathbf{D}$ and $\mathbf{V} = \mathbf{E}$.

The points $\mathbf{P}_u$, $\mathbf{D}_u$, and $\mathbf{E}_u$ are constant, since $\mathbf{P}$, $\mathbf{D}$, and $\mathbf{E}$ are fixed with respect to the wedge, but $\mathbf{P}$, $\mathbf{D}$, and $\mathbf{E}$ themselves are apt to depend on the wedge orientation u. The points $\mathbf{k}$ and $\mathbf{S}$ are fixed in space and are constant, but $\mathbf{k}_u$ and $\mathbf{S}_u$, which represent the zenith point and sun point as seen by the wedge rider, are apt to depend on u.

As the wedge takes on its various orientations and makes the halo, the point $\mathbf{k}_u$ traces out the *zenith locus* on the unit sphere. It is the path of the zenith point as seen by the wedge rider.

For a non-contact arc the spin vector $\mathbf{P}$ points directly up, and so $\mathbf{P} = \mathbf{k}$ and then $\mathbf{P}_u = \mathbf{k}_u$. Since $\mathbf{P}_u$ is independent of the wedge orientation u, so is $\mathbf{k}_u$. The zenith locus for a non-contact arc therefore consists of the single point $\mathbf{P}_u$, the pole of the arc.

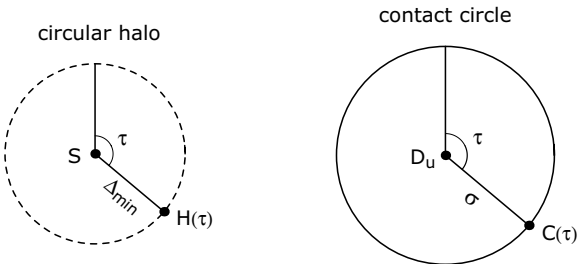

FIGURE F.2 Correspondence between the circular halo (dashed) and the contact circle. The circular halo has center at the sun **S** and has angular radius Δ_{min}. The contact circle has center at the minimum deviation point $\mathbf{D}_u$ and has angular radius equal to the solar zenith angle σ. The point $\mathbf{H}(\tau)$ is the point on the circular halo with bearing τ, and $\mathbf{C}(\tau)$ is the point on the contact circle with bearing τ. According to the criterion for contact, $\mathbf{H}(\tau)$ is a contact point for a given arc at a given solar zenith angle σ if and only if $\mathbf{C}(\tau)$ is on the zenith locus of the arc.

For a contact arc, the spin vector $\mathbf{P}$ is horizontal. Thus $\mathbf{P}$, which varies, remains orthogonal to the fixed point $\mathbf{k}$. But then $\mathbf{k}_u$, which now varies, is orthogonal to the fixed point $\mathbf{P}_u$. The zenith locus of a contact arc is the great circle with center at the pole $\mathbf{P}_u$.

With just a bit more terminology we can express the criterion for contact with the circular halo. The circular halo, or rather its inner boundary, is of course the circle on the unit sphere with center $\mathbf{S}$ and with angular radius Δ_{min}. The *contact circle* is the circle on the unit sphere with center $\mathbf{D}_u$ and angular radius equal to the solar zenith angle σ. We define $\mathbf{H}(\tau)$ to be the point on the circular halo with bearing τ, and $\mathbf{C}(\tau)$ to be the point on the contact circle with bearing τ (Figure F.2). Here we are using the term bearing in the sense of compass bearing, so that, for example, on a clock face the bearing of 3:00 would be 90°.

Criterion for contact *For a given refraction arc and a given solar zenith angle, the point* $\mathbf{H}(\tau)$ *on the circular halo is a contact point if and only if the point* $\mathbf{C}(\tau)$ *on the contact circle is on the zenith locus.*

Thus, to find the contact points of the arc at a given solar zenith angle σ, you just see where the contact circle intersects the zenith locus of the arc. The points of intersection correspond to contact points, with the disposition of the intersection points on the contact circle being the same as the disposition of the contact points on the circular halo.

If the halo is a non-contact arc the situation is simple (Figure F.3). The zenith locus consists of the single point $\mathbf{P}_u$, the pole of the arc. The contact circle passes

through $\mathbf{P}_u$ for only one σ, namely, $\sigma = s$, where s as usual is the angular distance from $\mathbf{D}_u$ to $\mathbf{P}_u$. Thus only when σ equals s does the arc contact the circular halo. In that case the direction of the contact point from the sun is the same as the direction of $\mathbf{P}_u$ from $\mathbf{D}_u$. This is as described in Chapter 14.

If the halo is a contact arc then the zenith locus is the great circle with center at $\mathbf{P}_u$. The dependence of the contact points on σ is illustrated in Figure F.4. The dependence is as described in Chapter 16.

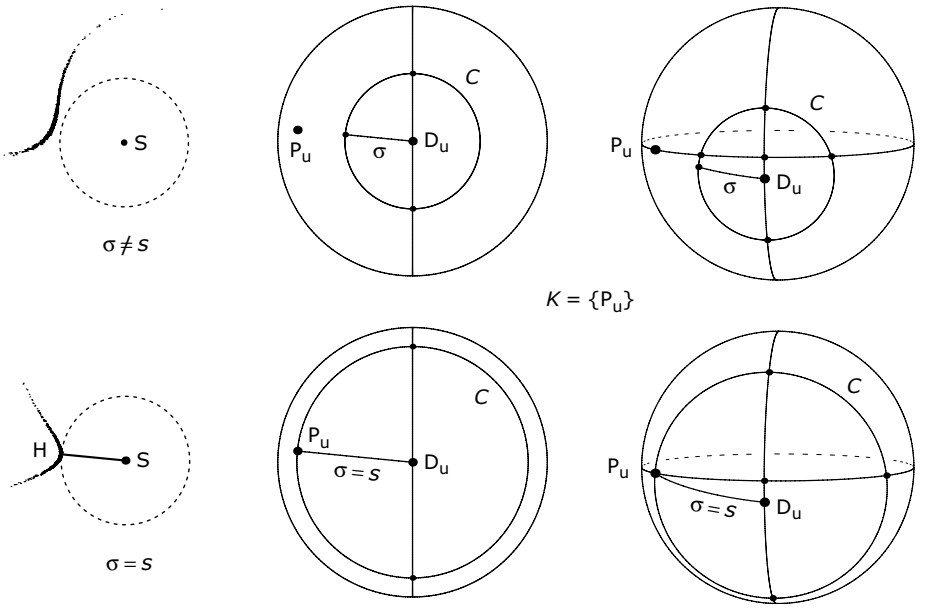

FIGURE F.3 Finding the contact point of a non-contact arc. Contact points always correspond to intersection points of the contact circle with the zenith locus, the correspondence being as in Figure F.2. Here a non-contact arc and its associated circular halo (dashed) are shown at left for two different solar zenith angles σ. The contact circle C and zenith locus K are shown in the middle diagram, as seen looking directly down at $\mathbf{D}_u$, and then again at the right, seen in the conventional perspective (Figure F.1, right). The circle C has center $\mathbf{D}_u$ and angular radius σ. Since the arc here is a non-contact arc, K consists of the single point $\mathbf{P}_u$, the pole of the arc. (*Top*) The case $\sigma \neq s$, where s is the angular distance from $\mathbf{D}_u$ to $\mathbf{P}_u$. The circle C misses K and so there are no contact points. (*Bottom*) The case $\sigma = s$. The circle C meets K at $\mathbf{P}_u$, so there is a single contact point $\mathbf{H}$, and the direction of $\mathbf{H}$ from the sun $\mathbf{S}$ is the same as the direction of $\mathbf{P}_u$ from $\mathbf{D}_u$. The halo here is the 18° plate arc with wedge 13 25, for which $s = 59°$. It is among the halos shown in Figure 15.6.

The two halos in Figures F.3 and F.4 have the same pole. Comparison of the two figures will explain the contrasting behavior of contact points for contact arcs and non-contact arcs.

To see why the criterion for contact should be correct, refer to Figure F.5. Suppose first that the point $\mathbf{H}(\tau)$ on the circular halo is a halo point $\mathbf{H}$ for some orientation of the wedge. Since the deviation is minimum, then $\mathbf{S}_u$ and $\mathbf{H}_u$ must coincide with $\mathbf{D}_u$ and $\mathbf{E}_u$, respectively. But the two configurations **kSH** and $\mathbf{k}_u\mathbf{S}_u\mathbf{H}_u$ are congruent, since they consist of the same three points (zenith point, sun point, and halo point), just seen from different viewpoints. Comparing the two configurations, we see that the angular distance of $\mathbf{k}_u$ from $\mathbf{D}_u$ must be σ, and the bearing of $\mathbf{k}_u$ from $\mathbf{D}_u$ must be τ. That is, $\mathbf{k}_u = \mathbf{C}(\tau)$, and so $\mathbf{C}(\tau)$ is indeed on the zenith locus.

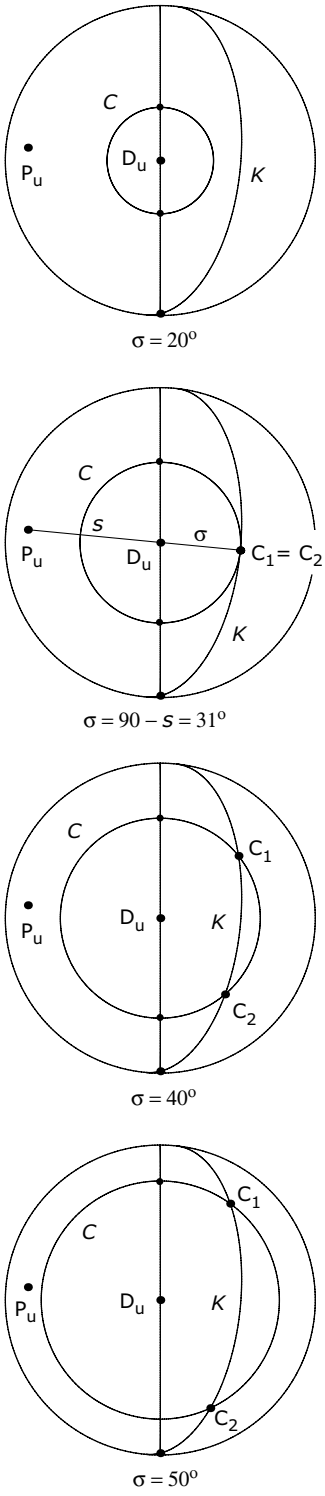

FIGURE F.4 Finding the contact points of a contact arc. Contact points correspond to intersection points $\mathbf{C}_1$ and $\mathbf{C}_2$ of the contact circle *C* with the zenith locus *K*. The circle *C* has center $\mathbf{D}_u$ and radius σ. For a contact arc, *K* is the great circle with center at the pole $\mathbf{P}_u$ of the arc. So here *K* is fixed but *C* shrinks as the solar zenith angle σ decreases. For large σ (*bottom*), that is, for low sun, there are two intersection points $\mathbf{C}_1$ and $\mathbf{C}_2$ of *C* with *K* and therefore two contact points. With decreasing σ the points $\mathbf{C}_1$ and $\mathbf{C}_2$—and therefore the contact points—move in the direction opposite the pole direction, until at $\sigma = 90 - s$ they merge into one as shown. For smaller σ (*top*) the circles *C* and *K* do not intersect, and there are no contact points. In each diagram the view is looking directly down on $\mathbf{D}_u$, the same as in the middle diagrams of Figure F.3. The halo here is the 18° column arc with wedge 13 25, for which $s = 59°$. The halo itself is shown in Figure 16.3. The $\Sigma = 40°$ and $\Sigma = 59°$ diagrams in that figure correspond to the $\sigma = 50°$ and $\sigma = 31°$ diagrams here.

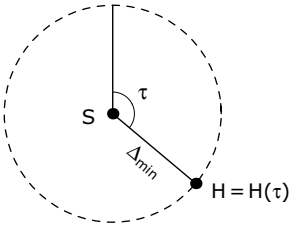

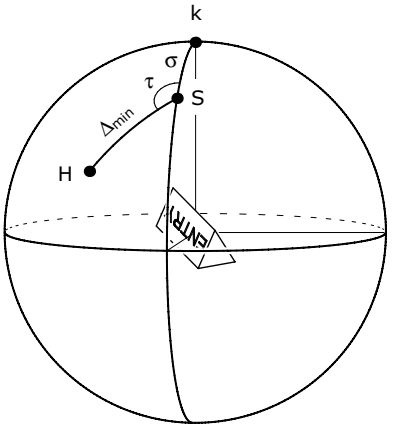

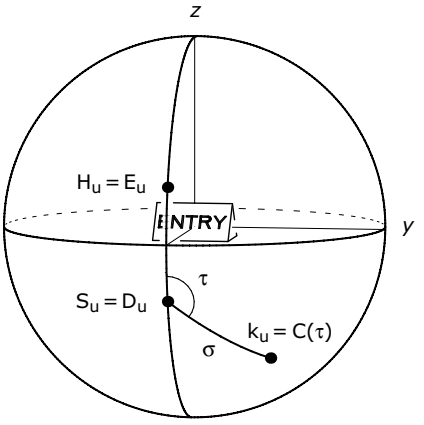

FIGURE F.5 Illustrating the criterion for contact. (*Top left*) A halo point $\mathbf{H} = \mathbf{H}(\tau)$ on the circular halo. The view is from inside the celestial sphere, as halos are seen in reality, and looking directly at the sun **S**. (*Top right*) The same points **H** and **S**, together with the zenith point **k**, but seen from outside the celestial sphere. The angular distance from **k** to **S** is the solar zenith angle σ. The responsible wedge is at the center of the sphere. (*Left*) Same as top right but showing the view from the wedge. That is, the entire configuration—sphere and wedge—has been rotated so that the wedge is now in standard orientation. Because the deviation is minimum, then $\mathbf{S}_u = \mathbf{D}_u$ and $\mathbf{H}_u = \mathbf{E}_u$. Since the bearing and angular distance of $\mathbf{k}_u$ from $\mathbf{D}_u$ are τ and σ, then $\mathbf{k}_u = \mathbf{C}(\tau)$. Thus $\mathbf{C}(\tau)$ is on the zenith locus.

Conversely, suppose the point $\mathbf{C}(\tau)$ on the contact circle is also on the zenith locus. Then $\mathbf{C}(\tau) = \mathbf{k}_u$ for some wedge orientation u. As the wedge rotates about the vertical axis in space,[1] the point $\mathbf{k}_u$ remains fixed, but $\mathbf{S}_u$, which must be at an angular distance of σ from $\mathbf{k}_u$, traces out the circle of radius σ centered at $\mathbf{k}_u$. Since the fixed point $\mathbf{D}_u$ is also at distance σ from $\mathbf{k}_u$, then at some moment the point $\mathbf{S}_u$ coincides with $\mathbf{D}_u$, in which case $\mathbf{H}_u$ coincides with $\mathbf{E}_u$. As before, the triangles $\mathbf{k}_u\mathbf{S}_u\mathbf{H}_u$ and $\mathbf{kSH}$ are congruent, so that $\mathbf{H} = \mathbf{H}(\tau)$. That is, the point $\mathbf{H}(\tau)$ on the circular halo is a halo point.

A careful reading of the preceding two paragraphs will show that the arc mentioned in the statement of the criterion for contact plays no role in the proof. The criterion is really a criterion for deciding when a point on the circular halo locus is in fact lit.

Well, that was a bit heavy. Let's end with something lighter, an exercise that you can do by living on the wedge: See if you can explain why non-contact arcs whose poles are on the equator must have their contact points on the parhelic circle. Hint: redraw Figure F.5 but with the point $\mathbf{k}_u = \mathbf{P}_u$ on the equator.

[1] Thus we are assuming: If a given wedge orientation is allowable, then so is any wedge orientation that results from the given one by a rotation about the vertical axis. This very mild assumption is satisfied by all of the usual crystal orientation classes and, more generally, by any crystal orientation class that is characterized by a spin vector.